scientific reports

Check for updates

OPEN

Wind dynamic environment, sand material transport law and prevention strategies of Sichuan Tibet Railway

Shengbo Xie[1]✉, Keying Zhang[1,2], Xian Zhang[1,2] & Kecun Zhang[1]

The Sichuan-Tibet Railway passes through windy and sandy areas in the river valleys of the southern Tibetan Plateau. Currently, the wind dynamic environment, sand material characteristics, and transport laws along the route are not well understood, hindering targeted sand control efforts. Through installing meteorological stations in the four wind-sand hazard sections along the route, respectively, key factors such as wind speed, wind direction and humidity that affect the dynamic process of wind-sand were observed, and sand samples were collected for particle size analysis. It is found that the average wind speed, sand-moving wind frequency, sand drift potential (DP), resultant drift potential (RDP), maximum possible sand transport quantity (Q), and resultant maximum possible sand transport quantity (RQ) are highest in spring (February to April). The predominant wind directions throughout the year are E, SSE, and ENE. Overall, the railway line is characterized by a low wind energy environment (DP ≤ 200 VU), and the directional variability index is moderate (0.3 < RDP/DP < 0.8). Sand materials are primarily fine sand (2–3 Φ) and medium sand (1–2 Φ). The key period for wind-sand hazard prevention and control is spring. The wind-sand prevention and control of the railway should focus on blocking (sand) and consolidating (sand), using external barriers and internal consolidation (distant blocking and near consolidation). Simultaneously, sand-fixing vegetation should be cultivated to establish a comprehensive protection system. To ensure the smooth operation of railway and the safety of train operation. The findings provide a scientific basis for the prevention and control of wind-sand hazards along the Sichuan-Tibet Railway.

Keywords Sichuan-Tibet railway, Wind dynamic environment, Sand transport, Sand prevention technology

The Sichuan–Tibet Railway is situated in southwest China, extending from Chengdu in Sichuan Province in the east to Lasa in the Tibet Autonomous Region in the west, with an approximate total length of 1,550 km (Fig. 1). This railway constitutes a vital trunk line within China's transportation network. Construction commenced in 2014, and to date, the Chengdu–Ya'an and Lasa–Linzhi sections have been completed, while the Ya'an–Linzhi section remains under construction. The topography of the Sichuan–Tibet Railway is characterized by complex mountainous and canyon formations, a diverse climate, variable weather patterns, a fragile ecological environment, and frequent natural disasters[1,2]. Notably, wind-sand events represent significant natural hazards, particularly concentrated in the southern Tibetan river valley section (Fig. 1)[3–5]. Contributing factors to these events include a dry and windy climate, abundant sand material sources, sparse and low vegetation, a short growing season, and heightened human activities, which collectively exacerbate desertification in the southern Tibetan river valley[6–8]. The region exhibits typical wind-sand landforms[9–12], including extensive mobile sand dunes and sandy terrain along the railway corridor[13–15]. The intensity of wind-sand activities poses a severe threat to railway infrastructure[16]. Moreover, the construction of the railway has inevitably led to the destruction of sparse vegetation and the disruption of fragile ecological systems along the route. The accumulation of wind-sand flow and the forward movement of sand dunes have resulted in the railway obstructing the pre-existing wind-sand transport processes on the surface[17], thereby altering the operational pathways and intensity of near-surface wind-sand flows[18,19], thereby exacerbating wind-sand hazards.

[1]Key Laboratory of Ecological Safety and Sustainable Development in Arid Lands / Dunhuang Gobi and Desert Research Station, Northwest Institute of Eco–Environment and Resources, Chinese Academy of Sciences, Lanzhou 730000, China. [2]University of Chinese Academy of Sciences, Beijing 100049, China. ✉email: xieshengbo@lzb.ac.cn

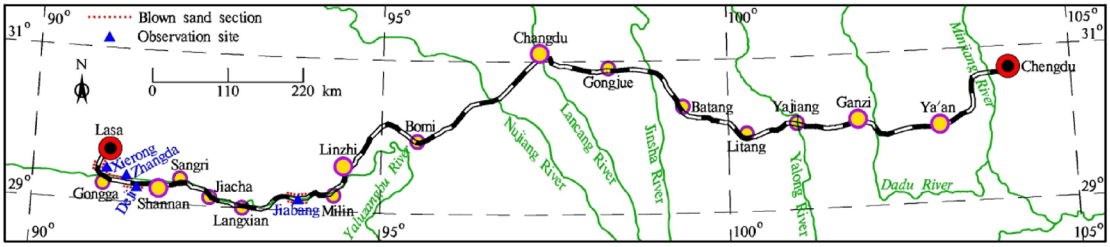

Fig. 1. Schematic diagram of the Sichuan-Tibet Railway and its sandy sections.

Observation location	Longitude	Latitude	Altitude	Average annual temperature
Xierong	90°54'33"E	29°22'45"N	3612 m	11.18 ℃
Zhangda	91°18'31"E	29°18'18"N	3581 m	11.13 ℃
Deji	91°31'14"E	29°15'39"N	3562 m	11.02 ℃
Jiabang	93°46'19"E	29°08'13"N	2988 m	11.00 ℃

Table 1. Overview of four observation points along the Sichuan-Tibet Railway.

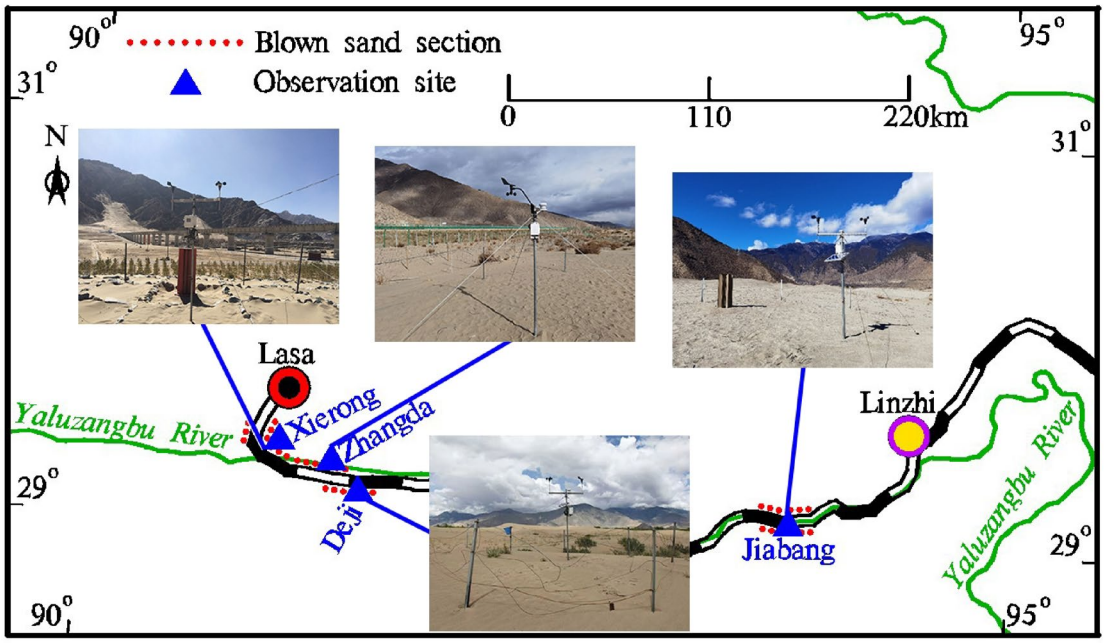

Fig. 2. Photos of four observation points along the Sichuan-Tibet Railway (The four photographs were taken by the first author Shengbo Xie).

The Sichuan-Tibet Railway was built in 2014 and has not been fully completed yet. It is a new railway line. Because the railway passes through windy and sandy areas in the river valleys of the southern Tibetan Plateau, it is severely affected by wind-sand hazards. However, the wind dynamic environment, the characteristics of sand materials and their transport laws along the route are currently unclear, hindering the implementation of scientifically effective wind-sand hazard mitigation measures. This investigation attempting to reveal the dynamic process and transport law of wind-blown sand along the Sichuan-Tibet Railway, thereby providing a scientific basis for the prevention and control of wind-sand hazards along the railway.

Research methods

Through field investigations, it was determined that wind-sand distribution along the Sichuan-Tibet Railway is concentrated in four distinct sections: Xierong in the Lasa River valley, Zhangda and Deji in the Shannan wide valley of the Yaluzangbu River, and Jiabang in the Milin wide valley of the Yaluzangbu River. These sections were subsequently designated as observation points (Table 1), where instruments were deployed (Fig. 2) to monitor

the local wind-sand environment. Additionally, sand samples were collected for particle size analysis utilizing a laser particle size analyzer. Each observation point is situated within typical wind-sand regions of the river valleys on the southern Tibetan Plateau.

The HOBO Automatic Meteorological Station was installed to observe the wind speed and wind direction. The wind speed was measured by using the S-WSET-B sensor, which has an operating range of 0 $m{\cdot}s^{-1}$ to 76 $m{\cdot}s^{-1}$ and accuracy of 0.5 $m{\cdot}s^{-1}$. Meanwhile, the wind direction was measured by using the S-WDA-M003 sensor, which has an operating range of 0° to 360° and accuracy of 1.4°, and HOBOware Pro was used as the control software. Following relevant studies[20,21], meteorological sensors were installed at a surface height of 2 m to record the wind speed and wind direction in the aforementioned four observation points every 5 min from November 2023 to October 2024.

Based on the observational data, firstly, wind condition indicators, such as average wind speed, sand-moving wind frequency, wind rose, and sand-moving wind rose were statistically analyzed, to elucidate the wind dynamic environment of the Sichuan-Tibet Railway. Subsequently, various wind-sand transport indicators, such as sand drift potential (DP), resultant drift potential (RDP), resultant drift direction (RDD), maximum possible sand transport quantity (Q), resultant maximum possible sand transport quantity (RQ), and the resultant angle of the maximum possible sand transport quantity (RA) were calculated, to investigate the sand transport dynamics along the Sichuan-Tibet Railway.

The calculation method of sand DP is as follows[22]:

$$DP = V^2(V - V_t)t \tag{1}$$

Where: DP is the sand drift potential, expressed in VU (vector unit); V is the wind speed greater than the critical starting value ($m{\cdot}s^{-1}$); V_t is the critical starting wind speed ($m{\cdot}s^{-1}$), taken as 5.0 $m{\cdot}s^{-1}$; t is the sand-moving wind action time. The sand DP is synthesized according to the vector synthesis rule to obtain RDP (VU) and RDD (°), and RDP/DP is the directional variability index.

The maximum possible sand transport quantity is calculated as follows[23]:

$$Q = 8.95 \times 10^{-1}(V - V_t) \times T \tag{2}$$

Where: Q is the maximum possible sand transport quantity ($kg{\cdot}m^{-1}{\cdot}a^{-1}$); V is the wind speed greater than the critical starting value ($m{\cdot}s^{-1}$); V_t is the critical starting wind speed ($m{\cdot}s^{-1}$), which is 5.0 $m{\cdot}s^{-1}$; T is the cumulative duration of wind speeds of different levels. The maximum possible sand transport quantity is synthesized according to the vector synthesis rule to obtain RQ ($kg{\cdot}m^{-1}{\cdot}a^{-1}$) and RA (°).

Results and analysis

Average wind speed and sand-moving wind frequency

In Xierong, the average wind speed reaches its peak in June at 2.24 $m{\cdot}s^{-1}$, while it is at its lowest in November, measuring only 1.09 $m{\cdot}s^{-1}$, resulting in an annual average of 1.66 $m{\cdot}s^{-1}$. The frequency of sand-moving winds is highest in April, at 8.49%, and lowest in November, at merely 1.44%, yielding an annual frequency of 4.55%.

In Zhangda, the average wind speed peaks in February at 2.86 $m{\cdot}s^{-1}$, with a minimum of 1.49 $m{\cdot}s^{-1}$ recorded in December, leading to an annual average of 2.14 $m{\cdot}s^{-1}$. The frequency of sand-moving winds also peaks in February at 15.29%, while it declines to 2.50% in November, resulting in an annual frequency of 6.36%.

In Deji, the highest average wind speed occurs in March, measuring 2.43 $m{\cdot}s^{-1}$, with a low of 1.05 $m{\cdot}s^{-1}$ in November, culminating in an annual average of 1.73 $m{\cdot}s^{-1}$. The frequency of sand-moving winds is maximized in March at 17.31%, and minimized in November at 4.05%, producing an annual frequency of 9.05%.

In Jiabang, the highest average wind speed is recorded in March at 3.23 $m{\cdot}s^{-1}$, while the lowest occurs in November at 2.14 $m{\cdot}s^{-1}$, resulting in an annual average of 2.60 $m{\cdot}s^{-1}$. The frequency of sand-moving winds peaks in March at 25.55% and is lowest in July at 9.48%, leading to an annual frequency of 15.00% (Fig. 3).

As illustrated in Fig. 3, both the average wind speed and the frequency of sand-moving winds along the Sichuan-Tibet Railway are elevated during the spring months and reduced in winter, with intermediate levels observed in summer and autumn. The seasonal fluctuations in both parameters demonstrate a consistent pattern.

Wind rose

The predominant wind direction in Xierong is from the southeast-south (SSE), comprising 10.35% of the annual total, followed by the southeast-east (ESE) wind, which accounts for 8.35% of the total. The frequency of calm conditions is noted at 22.45%.

In Zhangda, the prevailing wind direction is from the east (E), representing 16.48% of the annual total, succeeded by the ESE wind, which constitutes 15.19% of the total. The frequency of static wind conditions is recorded at 8.53%.

The annual wind direction at Deji is predominantly influenced by the northeast-east (ENE) wind, which constitutes 10.91% of the total annual wind frequency. This is followed by the east (E) wind, accounting for 7.82% of the annual total, while static winds represent 28.31% of the occurrences.

The annual wind direction at Jiabang is primarily driven by the southeast-south (SSE) wind, which comprises 25.48% of the total annual frequency. The south (S) wind accounts for 17.32% of the annual total, and the frequency of static winds is recorded at 16.64% (Fig. 4).

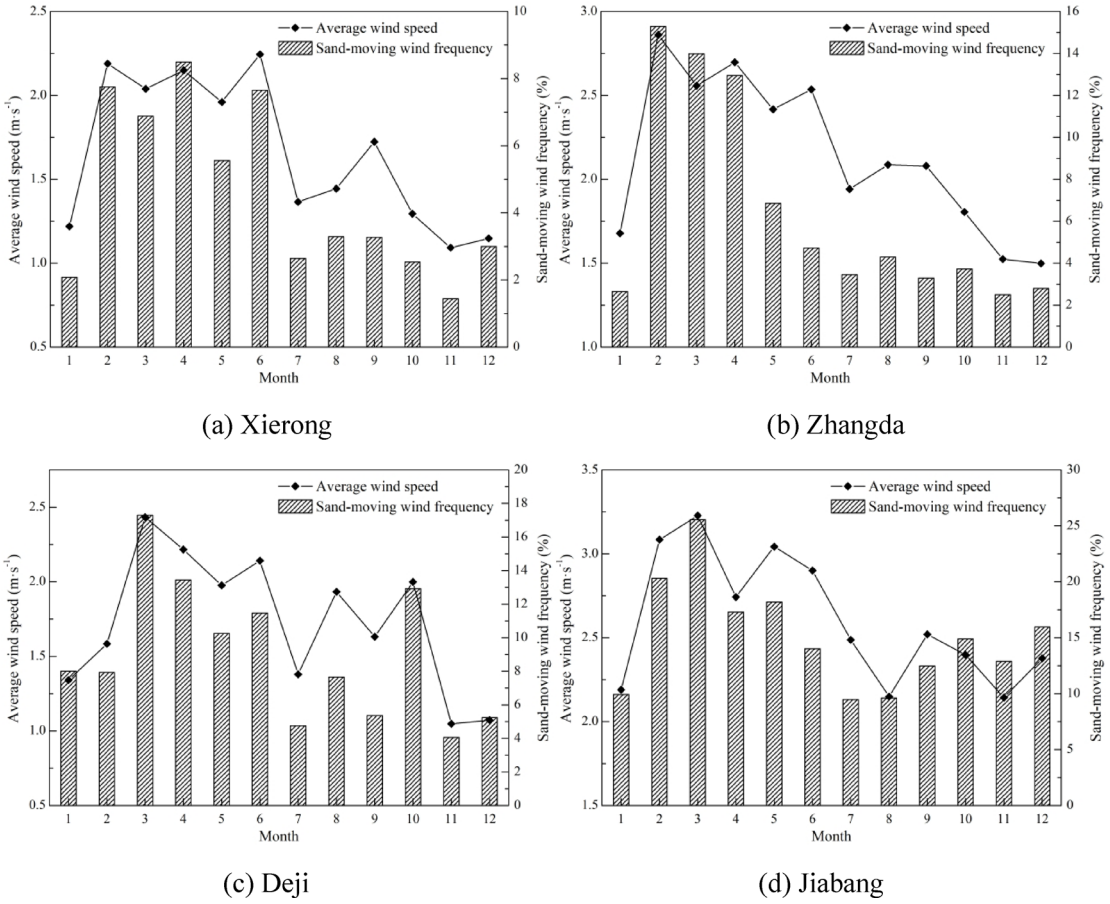

Fig. 3. Annual changes in average wind speed and sand-moving wind frequency at each observation point.

Sand-moving wind rose

The predominant sand-moving wind direction at Xierong is the northeast-north (NNE) wind, which constitutes 25.66% of the annual total, followed by the SSE wind at 20.23%. The annual resultant sand-moving wind direction is measured at 98.72°, indicating an easterly direction.

At Zhangda, the sand-moving wind is chiefly characterized by the west (W) wind, which accounts for 32.10% of the annual total, followed by the ESE wind at 17.42%. The annual resultant sand-moving wind direction is 267.70°, corresponding to the west.

In Deji, the sand-moving wind direction is dominated by the ENE wind, representing 28.57% of the annual total, with the E wind following at 25.83%. The annual resultant sand-moving wind direction is recorded at 76.33°, indicating an ENE direction.

Finally, Jiabang exhibits a sand-moving wind direction predominantly influenced by the SSE wind, which constitutes 22.74% of the annual total, followed by the ESE wind at 19.48%. The annual resultant sand-moving wind direction is measured at 136.58°, corresponding to a southeast direction (Fig. 5).

Sand DP

During the spring months (February to April), both the DP and RDP at Xierong are elevated, peaking in April with DP and RDP values of 4.40 VU and 3.42 VU, respectively, which correspond to 22.83% and 38.38% of the annual totals. Conversely, during the winter months (November to January), both DP and RDP values are relatively low, with a dispersed RDD. In October, the RDP/DP ratio exceeds 0.8, indicating a significant proportion ($RDP/DP \geq 0.8$), while in the remaining months, the ratio fluctuates between 0.3 and 0.8, classifying it as a moderate ratio ($0.3 < RDP/DP < 0.8$).

In the spring months (February to April), both the DP and RDP at Zhangda exhibit elevated values, peaking in February with DP and RDP recorded at 14.66 VU and 13.29 VU, respectively. These values represent 36.24% and 45.50% of the annual totals. In contrast, DP and RDP are notably lower during other seasons. The RDD predominantly trends eastward during winter and spring (November to April), while it becomes more dispersed in summer and autumn (May to October). Notably, during December and from February to April, the ratio of RDP to DP exceeds 0.8, indicating a significant proportion, whereas in other months, this ratio falls below 0.8, indicating a moderate to low ratio. This observation suggests a consistent wind direction in Zhangda during the spring months.

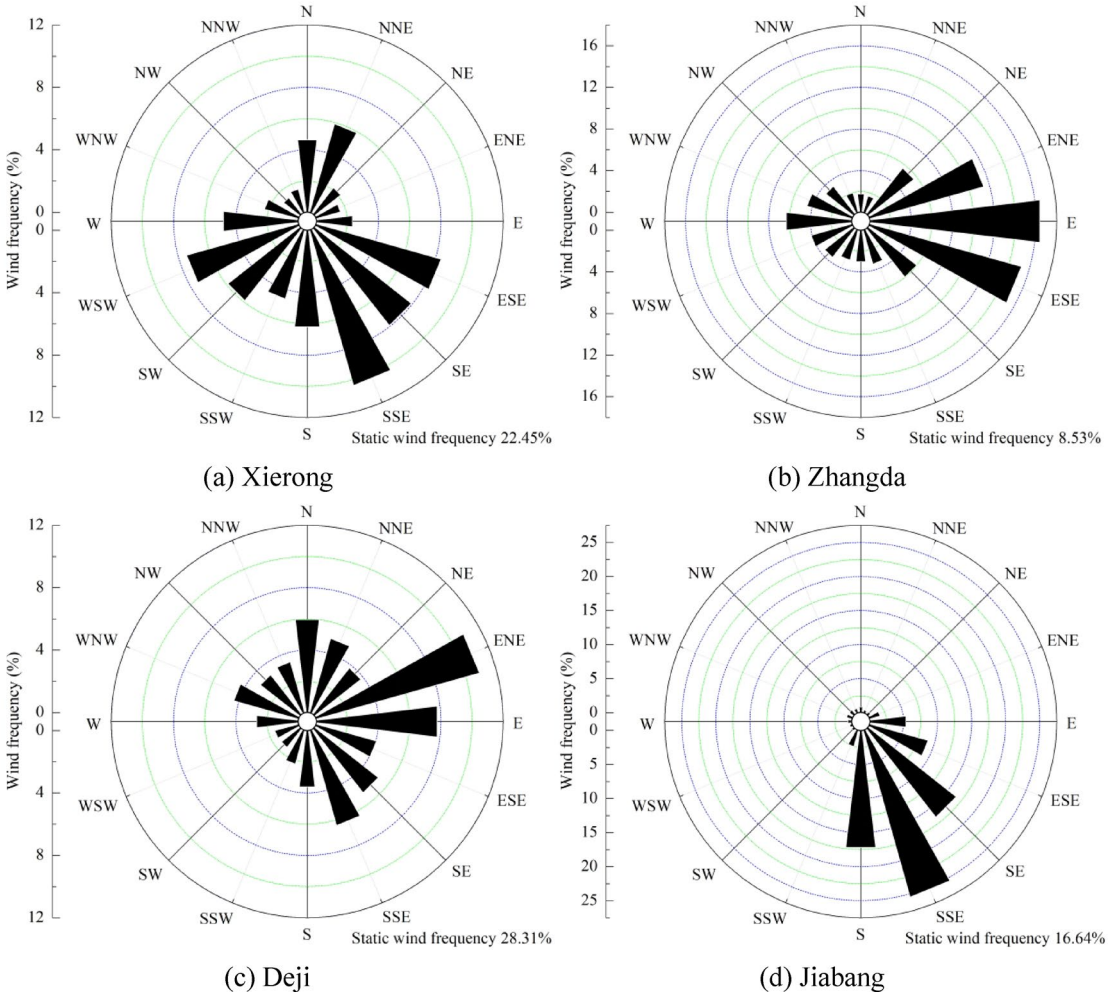

Fig. 4. Annual wind rose diagrams of each observation point.

In spring (February to April), the DP of Deji is high, with March recording the highest value of 7.52 VU, which constitutes 19.45% of the annual total. Conversely, both DP and RDP are lower during winter (November to January). The RDD remains dispersed throughout the year, with the ratio of RDP to DP being higher in summer and autumn and lower during winter and spring, indicating a more variable wind direction in Deji during the latter seasons.

In spring (February to April), the DP and RDP of Jiabang are high, with February marking the peak at 7.67 VU and 6.59 VU, respectively, accounting for 15.75% and 18.78% of the annual totals. During other seasons, both DP and RDP remain relatively low. The RDD predominantly aligns with the WNW, NW, and NNW directions. The RDP/DP ratio in February, March, October, and December exceeds 0.8, indicating a significant ratio, while in the remaining months, it ranges from 0.3 to 0.8, reflecting a moderate ratio (Fig. 6; Table 2).

The annual DP for Xierong is recorded at 19.72 VU, with an annual RDP of 8.91 VU and an RDP/DP ratio of 0.45, indicating a moderate ratio. The annual RDD is 221.72°, oriented southwest.

For Zhangda, the annual DP is measured at 40.45 VU, with an annual RDP of 29.21 VU, resulting in an RDP/DP ratio of 0.72, which is also classified as moderate. The annual RDD is 92.70°, directed eastward.

The annual DP at Deji is recorded at 47.40 VU, while the annual RDP stands at 15.32 VU. The ratio of RDP to DP is 0.32, indicative of a medium ratio, and the annual RDD is measured at 248.82°, corresponding to a southwest-west (WSW) orientation.

Jiabang exhibits an annual DP of 48.69 VU and an annual RDP of 35.09 VU. The RDP/DP ratio is 0.72, also classified as a medium ratio, with an annual RDD of 307.82°, indicating a northwest (NW) direction (Fig. 7).

Sand transport quantity

In Xierong, Q and RQ peak during spring (February to April), reaching their maximum values in April at 9.00 $kg{\cdot}m^{-1}{\cdot}a^{-1}$ and 7.71 $kg{\cdot}m^{-1}{\cdot}a^{-1}$, respectively. These values constitute 24.58% and 37.43% of the annual totals, respectively. Conversely, Q and RQ are relatively diminished during the winter months (November to January). RA in winter is southwest-south (SSW), while it is dispersed across other seasons.

In Zhangda, Q and RQ are similarly elevated in spring (February to April), with peak values observed in February at 34.71 $kg{\cdot}m^{-1}{\cdot}a^{-1}$ and 32.56 $kg{\cdot}m^{-1}{\cdot}a^{-1}$, accounting for 39.62% and 46.05% of the annual totals,

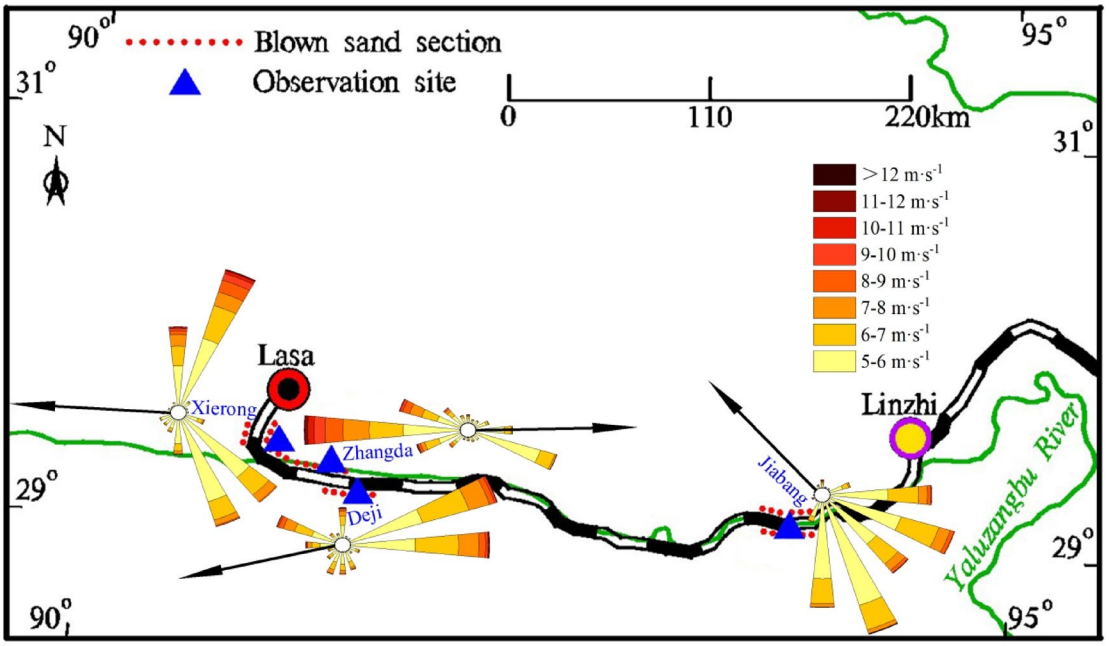

Fig. 5. Annual sand-moving wind rose diagrams of each observation point.

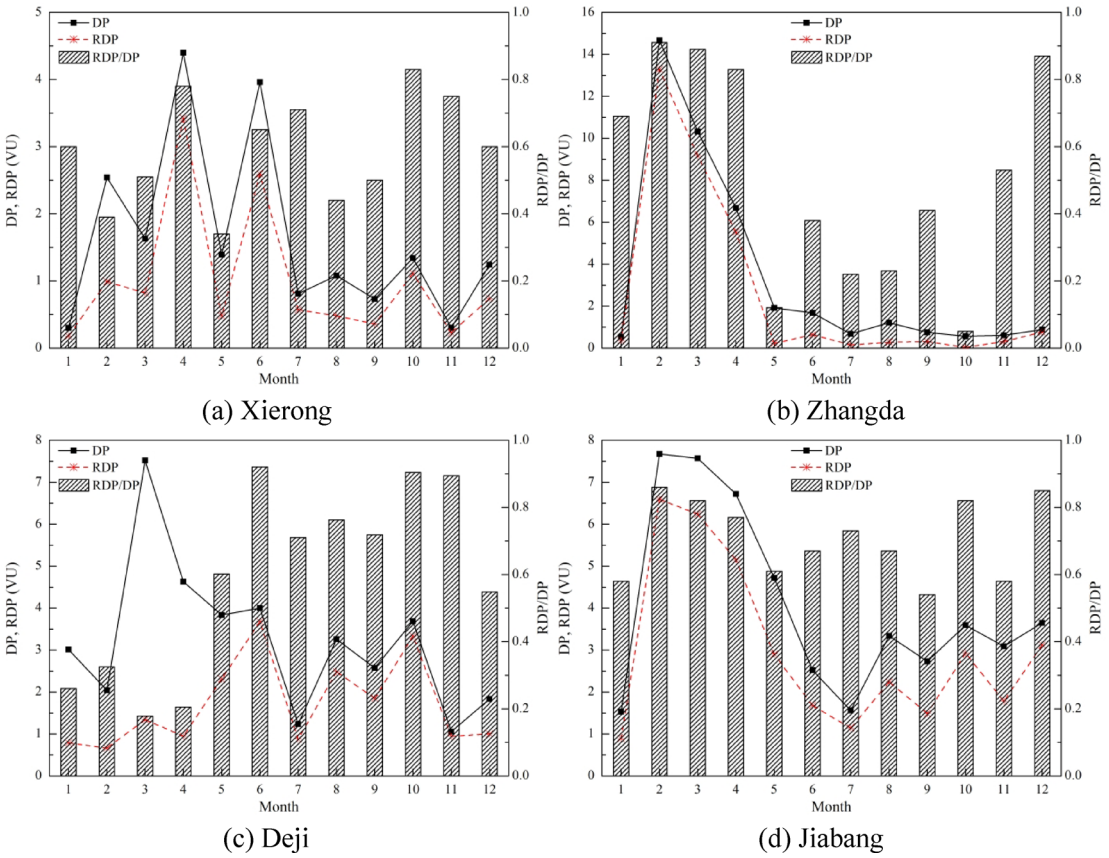

Fig. 6. Annual changes of sand DP at each observation point.

Month		1	2	3	4	5	6	7	8	9	10	11	12
Xie rong	RDD(°)	212.84	236.66	319.84	198.54	280.12	200.63	324.84	286.74	308.83	200.06	209.14	216.89
	Direction	SSW	WSW	NW	SSW	W	SSW	NW	WNW	NW	SSW	SSW	SW
	RA(°)	205.44	220.12	301.26	198.06	261.17	196.19	329.75	290.66	318.56	197.71	205.85	212.25
	Direction	SSW	SW	WNW	SSW	W	SSW	NNW	WNW	NW	SSW	SSW	SSW
Zhang da	RDD(°)	287.01	89.59	94.01	95.60	87.33	139.53	32.11	283.42	160.62	319.30	82.27	81.20
	Direction	WNW	E	E	E	E	SE	NNE	WNW	SSE	NW	E	E
	RA(°)	105.80	89.64	94.36	95.45	95.79	131.27	56.12	103.34	160.65	77.30	86.91	80.83
	Direction	ESE	E	E	E	E	SE	NE	ESE	SSE	ENE	E	E
Deji	RDD(°)	122.97	179.06	126.56	233.89	262.36	256.18	265.94	260.52	257.95	270.97	105.83	96.88
	Direction	ESE	S	SE	SW	W	WSW	W	W	WSW	W	ESE	E
	RA(°)	127.58	179.33	125.75	230.40	262.16	255.62	266.37	259.60	257.78	271.11	105.82	95.97
	Direction	SE	S	SE	SW	W	WSW	W	W	WSW	W	ESE	E
Jia bang	RDD(°)	325.18	300.46	295.07	296.48	297.47	316.32	332.73	328.61	300.70	329.96	310.48	325.78
	Direction	NW	WNW	WNW	WNW	WNW	NW	NNW	NNW	WNW	NNW	NW	NW
	RA(°)	316.56	296.99	290.53	294.47	293.32	316.61	336.21	334.26	277.67	329.08	296.35	323.16
	Direction	NW	WNW	WNW	WNW	WNW	NW	NNW	NNW	W	NNW	WNW	NW

Table 2. Annual changes in the sand resultant drift direction at each observation point.

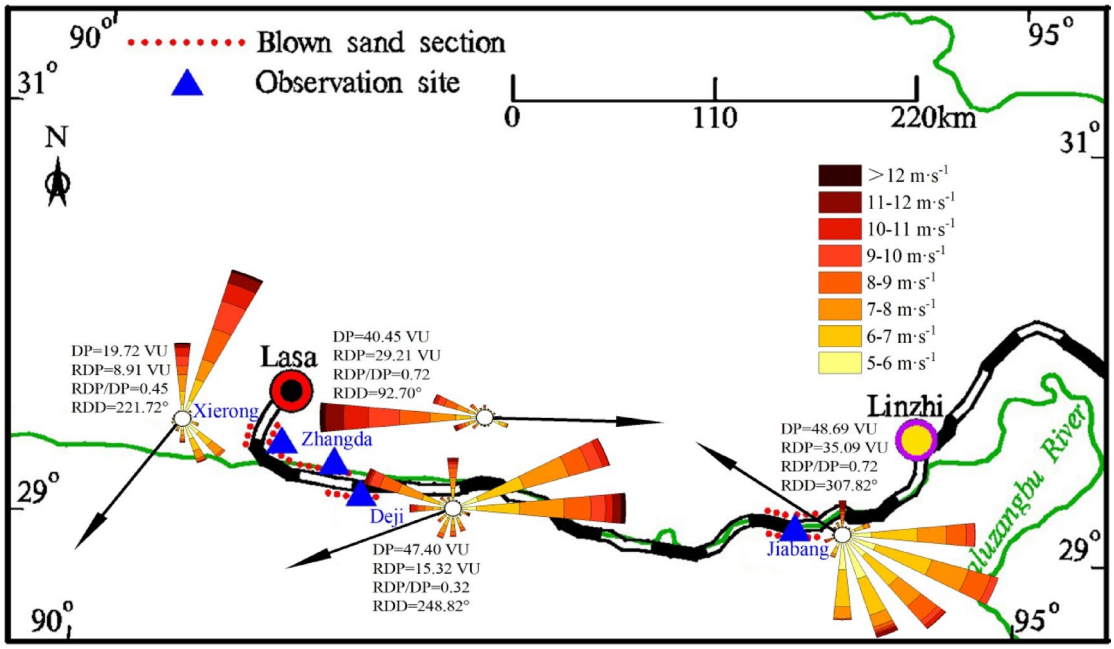

Fig. 7. Rose diagrams of annual sand DP at each observation point.

respectively. In contrast, Q and RQ are notably lower during other seasons. During the winter and spring months (November to April), RA predominantly aligns with the E direction, whereas in summer and autumn (May to October), RA becomes dispersed.

At Deji, Q and RQ also exhibit higher values during spring (February to April), peaking in March when Q reaches 18.37 $kg{\cdot}m^{-1}{\cdot}a^{-1}$, representing 19.91% of the annual total, while decline in winter (November to January). The RA is dispersed throughout the year.

In Jiabang, Q and RQ peak in spring (February to April), with maximum values recorded in February at 14.06 $kg{\cdot}m^{-1}{\cdot}a^{-1}$ and 12.37 $kg{\cdot}m^{-1}{\cdot}a^{-1}$, corresponding to 17.89% and 22.58% of the annual totals, respectively. Q and RQ are relatively low in other seasons. From November to April, RA is directed northwest-west (WNW) and northwest (NW), while in summer and autumn (May to October), RA is dispersed (Fig. 8; Table 2).

The annual Q for Xierong is quantified at 36.61 $kg{\cdot}m^{-1}{\cdot}a^{-1}$, with the wind force level contributing maximally distributed between 7 and 8 $m{\cdot}s^{-1}$. The annual RQ is recorded at 20.60 $kg{\cdot}m^{-1}{\cdot}a^{-1}$, and the annual RA is measured at 212.15°, corresponding to a SSW direction.

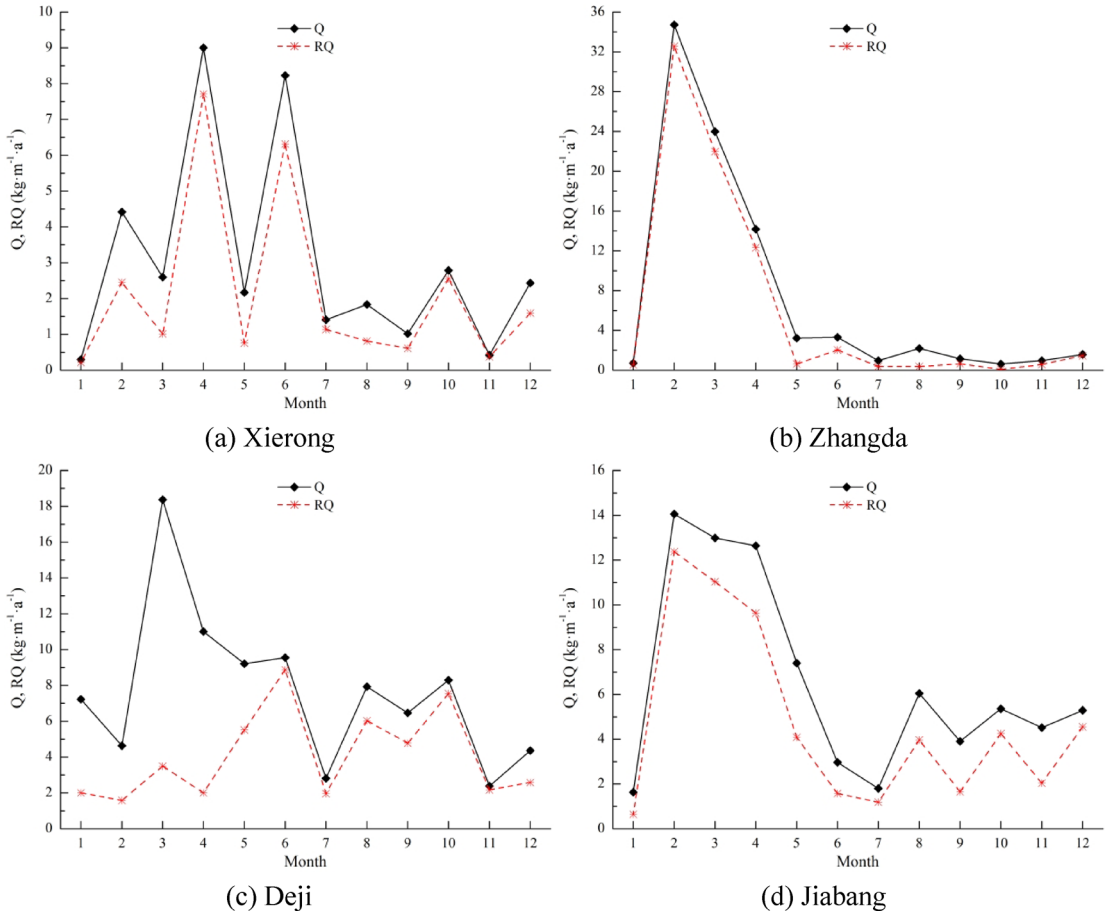

Fig. 8. Annual changes in the maximum possible sand transport quantity at each observation point.

The annual Q at Zhangda is quantified at 87.60 $kg{\cdot}m^{-1}{\cdot}a^{-1}$, with the predominant wind force contributing to this value occurring within the range of 8 to 9 $m{\cdot}s^{-1}$. The annual RQ is recorded at 70.71 $kg{\cdot}m^{-1}{\cdot}a^{-1}$, while the annual RA is measured at 93.19°, indicating an easterly direction.

At Deji, the annual Q is determined to be 92.25 $kg{\cdot}m^{-1}{\cdot}a^{-1}$, with the most significant wind force contributions occurring between 7 and 8 $m{\cdot}s^{-1}$. The annual RQ is assessed at 29.18 $kg{\cdot}m^{-1}{\cdot}a^{-1}$, and the annual RA is reported at 245.69°, corresponding to a WSW direction.

For Jiabang, the annual Q is calculated at 78.58 $kg{\cdot}m^{-1}{\cdot}a^{-1}$, with the dominant wind force occurring in the range of 6 to 7 $m{\cdot}s^{-1}$. The annual RQ is noted as 54.78 $kg{\cdot}m^{-1}{\cdot}a^{-1}$, while the annual RA is indicated at 302.93°, which aligns with a WNW direction (Fig. 9; Table 3).

Characteristics of sand materials

Analysis of the mechanical composition of sand material along the railway (Table 4) reveals that each observation point predominantly consists of fine sand (2–3 Φ) and medium sand (1–2 Φ). The average proportion of fine sand along the railway is 48.85%, while medium sand comprises an average of 47.65%. The proportions of sand materials of other particle sizes are minimal.

From the perspective of particle size distribution frequency of sand materials along the railway (Fig. 10), the frequency curves for sand materials at each observation point exhibit a single-peaked distribution. The peak values for the particle frequency of sand materials at Xierong and Deji correspond to medium sand (1–2 Φ), whereas the peak values for Zhangda and Jiabang are associated with fine sand (2–3 Φ). The heterogeneity in particle distribution of sand materials across the observation points along the railway is found to be minimal.

Discussion on prevention and control strategies

Generally speaking, the strategies for wind-sand prevention and control of the transportation routes need to be determined based on the following factors: ① The time period when wind-sand hazards occur. ② The grade of local wind energy environment, and the grade of protective and control measures in areas with a high wind energy grade should be correspondingly raised. ③ The resultant sand transport direction, i.e. the overall moving direction of sand materials, so as to set targeted prevention and control measures in the upwind direction. ④ The angle between the route alignment and the wind-sand transport direction, the smaller the angle, the lighter the degree of wind-sand hazards. ⑤ The size of sand particles, small particles are more likely to be triggered and are the key targets for sand prevention and control. In this study, the above five issues were resolved through

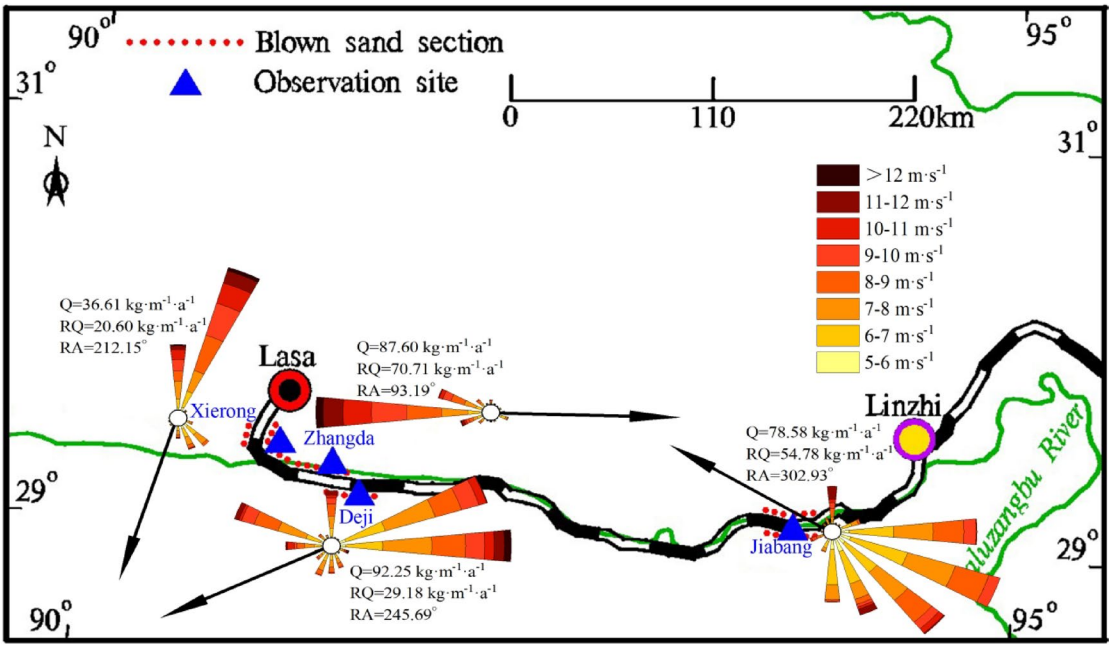

Fig. 9. Rose diagrams of the annual maximum possible sand transport quantity at each observation point.

Wind force level (m·s^{-1})		5–6	6–7	7–8	8–9	9–10	10–11	11–12	12–13	13–14
Q (kg·m^{-1}·a^{-1})	Xierong	1.70	6.84	8.58	7.13	5.75	4.00	2.00	0.37	0.24
	Zhangda	2.42	11.39	17.39	19.92	15.65	10.83	7.54	1.75	0.71
	Deji	2.98	21.05	28.72	19.39	10.41	4.79	3.51	0.91	0.47
	Jiabang	6.24	27.55	20.97	13.89	5.60	1.82	2.50	-	-

Table 3. Maximum possible sand transport quantity at each observation point and each wind force level.

Sampling location	Very coarse sand -1～0 Φ	Coarse sand 0～1 Φ	Medium sand 1～2 Φ	Fine sand 2～3 Φ	Very fine sand 3～4 Φ	Silt 4～8 Φ	Clay >8 Φ
Xierong	0.30	0.40	74.30	24.10	0.40	0.50	0
Zhangda	0	2.60	33.10	59.10	4.70	0.50	0
Deji	0	0.30	52.60	45.80	1.20	0.10	0
Jiabang	0	0.20	30.60	66.40	2.40	0.40	0
Average	0.075	0.875	47.65	48.85	2.175	0.375	0

Table 4. Particle gradation of sand material at each observation point (%).

field observations and the analysis and testing of sand samples. Among them, field observations identified four factors: the time period when railway wind-sand hazards occur, the grade of wind energy environment, the resultant sand transport direction, and the railway-wind angle. The analysis and testing of sand samples determined the particle size of sand materials.

The sandy regions adjacent to the Sichuan-Tibet Railway exhibit a plateau temperate semi-arid climate, characterized by an average annual precipitation ranging from 324 to 430 mm, with over 80% of this precipitation occurring during the summer and autumn months[24,25]. Based on the field observation results, the average wind speed, frequency of sand-moving winds, sand DP, and quantity of sand transport in spring show high values. Analysis of concurrently monitored temperature and humidity data (Fig. 11) reveals that air humidity during the winter and spring months is significantly lower than that observed in the summer and autumn, resulting in arid conditions, diminished surface water content, lowered river water levels, and exposed sand during the winter and spring seasons[14]. Notably, in spring, as the transition occurs from the cold season to the warm season, the ground surface undergoes a transformation from a frozen state to a thawed condition, becoming loose and fragmented, which increases its susceptibility to the mobilization of sand and dust[26,27]. Therefore, spring emerges as a critical period for the prevention and mitigation of wind-sand hazards along the Sichuan-Tibet Railway.

Based on the calculation results of the DP, the sandy regions along the Sichuan-Tibet Railway is characterized by a low wind energy environment (DP ≤ 200 VU), and the directional variability index is moderate (0.3 < RDP/

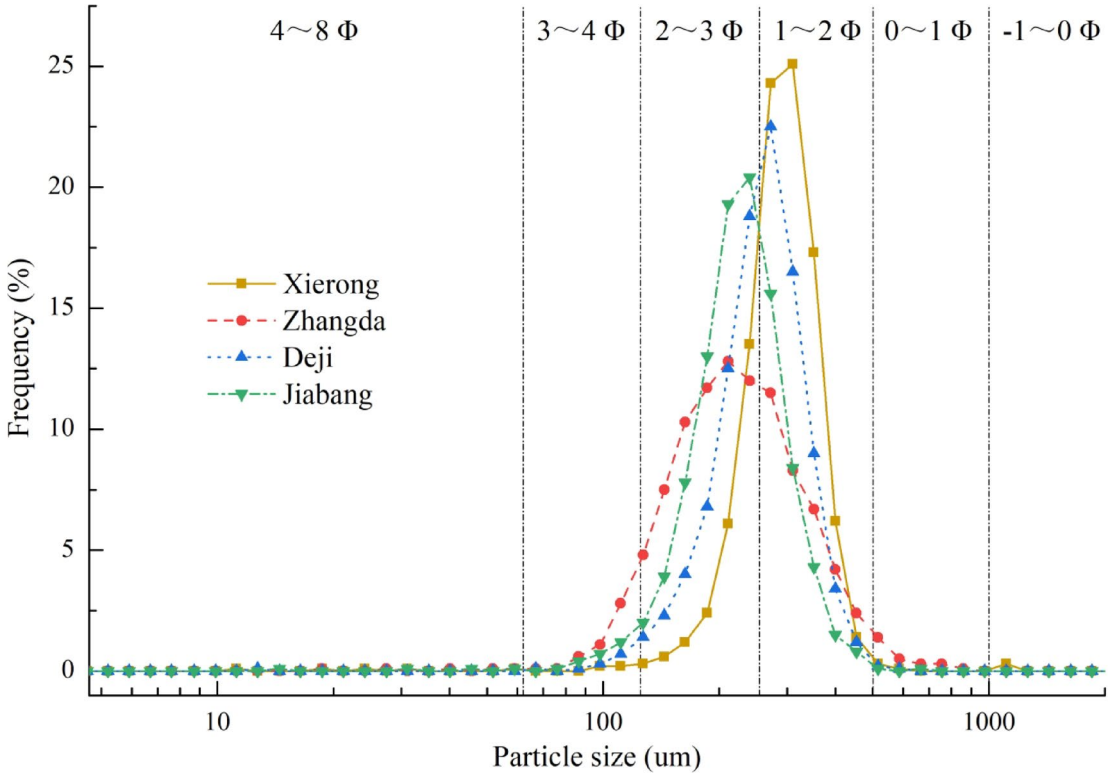

Fig. 10. Distribution frequency of sand materials particle size at each observation point.

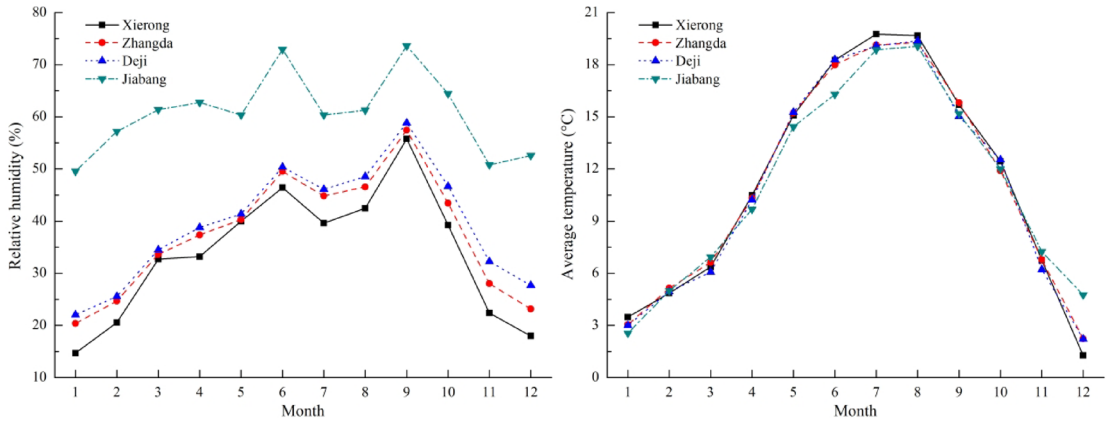

Fig. 11. Annual changes in temperature and humidity at each observation point.

DP < 0.8). Based on the aforementioned wind-sand transport direction relative to the railway alignment, the railway-wind angles for the four sections have been determined (Table 5). The main wind direction (west and east) in Xierong and the main wind direction (southwest) in Zhangda are consistent with the wind condition observed in the middle reaches of the Yaluzangbu River[28]. The annual sand transport potential at Jiabang (48.69 VU) is similar to that at Milin (34.52 VU) in a comparable area[29], and the annual sand-moving wind in Milin is from the southeaster[30], which is in the same direction as that of the study area. Overall, the wind direction in the study area is more complex, with significant seasonal variations, showing the highest average wind speed, frequency of sand-moving wind, and sand transport quantity in spring, which is similar to the study of the near-surface wind environment of the Yaluzangbu River[31,32]. Research indicates that a greater angle between the railway direction and the wind-sand transport direction correlates with increased severity of wind-sand damage[33,34]. Specifically, when the railway-wind angle is less than 30°, the detrimental impact of wind-sand on the railway can be effectively mitigated[35].

Considering the above observation results comprehensively, in the Zhangda and Deji sections, the wind-sand transport direction is nearly parallel to the railway alignment or the angle is small, resulting in a low degree of

Wind-sand section	Wind-sand transport direction ($N=0^o$)		Railway direction (°) ($N=0^o$)	Railway-wind angle (°)
	RDD(°)	RA(°)		
Xierong	221.7	212.2	11.5	20.7–30.2
Zhangda	92.7	93.2	92.6	0.1–0.6
Deji	248.8	245.7	81.9	13.1–16.2
Jiabang	307.8	302.9	83.8	39.1–44.0

Table 5. Railway-wind angle on sandy sections of Sichuan-Tibet Railway.

damage; therefore, no special sand control measures are deemed necessary. Instead, efforts should focus on closing and cultivating areas along the line to protect ecological integrity and restore vegetation. Conversely, the Xierong and Jiabang sections exhibit larger railway-wind angles, leading to significant wind-sand damage. Therefore, wind-sand prevention and control strategies in these sections should prioritize external blockades and internal consolidation, employing a dual approach of distant blocking and near consolidation. Concurrently, the cultivation of sand-fixing vegetation is essential to establish a comprehensive protection system. In the eastern side of Xierong section, a sand-blocking belt is established along the outer edge of the railway, this belt incorporates a high vertical concrete sand-blocking fence, featuring varying air permeability coefficients, or a polyethylene (PE) net sand-blocking fence with different porosities. To accommodate the undulating terrain of the hillside sand dunes, a large checkered sand barrier made of PE netting is implemented to impede and stabilize sand movement, thereby reducing wind velocity and effectively preventing the displacement of loose sand. Concurrently, a water diversion channel and a water dam are constructed at both ends of the protection belt to facilitate water diversion and sand flushing, with the Xierong area serving as a bridge section that can be utilized for these purposes. The accumulated sand within the sand-blocking belt is subject to regular maintenance and removal. In the central region, a mixed sand-fixing belt is established. Initially, a semi-hidden grid-shaped sand barrier, comprising various types of grids including grass grids, stone grids, and PE net grids, is employed to stabilize mobile sands. Subsequently, sand-fixing vegetation which primarily consisting of native species such as Sophora moorcroftiana, Sophora viciifolia, Elymus dahuricus, Medicago sativa, Artemisia ordosica, are cultivated within the grid-shaped sand barrier. An inner sand-sealing and grass-cultivating belt is also implemented. During the initial phase of closure, sand-dwelling plants are nurtured to enhance artificial ecological restoration and promote vegetative recovery. In the later stages, the closure may be gradually relaxed based on prevailing conditions, allowing for limited grazing and mowing activities. The western side of the Xierong section, which is located in downwind direction of the resultant sand transport direction, does not require sand control measures. In the southern side of Jiabang section, a sand-fixing belt is established along the outer edge of the railway, incorporating a semi-concealed grid-patterned sand barrier, which consists of variously sized grass grids, stone grids, and PE net grids. Once the sand bed surface within the barrier achieves stability, sand-fixing species such as Sophora moorcroftiana and Sophora viciifolia are planted and cultivated. Additionally, a sand-sealing and grass-cultivating belt is established centrally, predominantly featuring herbaceous species, including Medicago sativa, Tibetan Artemisia ordosica. The process is further enhanced through rotational sealing and grazing, promoting artificial ecological restoration. On the inner edge, a mixed forest and grass belt is created, forming an ecological protection belt that amalgamates native trees, shrubs, and grasses such as Populus szechuanica var. tibetica, Juniperus chinensis, Sophora moorcroftiana, and Elymus dahuricus. The northern side of the Jiabang section, which is located in downwind direction of the resultant sand transport direction, does not require sand control measures.

Of course, the above research results and sand control strategies are based on one-year field observations, which is a relatively short period of time and may be some limitations on the generalizability of the conclusions. At present, field observations of this study are still ongoing, multi-year observations data should be needed to enhance the generalizability of the conclusions in the following research.

Conclusions

Based on one-year field observations, this study investigated the wind dynamic environment, sand material transport law and prevention strategies of Sichuan-Tibet Railway, the following preliminary conclusions can be drawn under these experimental conditions:

The average wind speed, frequency of sand-moving winds, DP, RDP, Q, and RQ along the Sichuan-Tibet Railway are notably elevated during the spring months (February to April), with prevailing annual wind directions predominantly from the E, SSE, and ENE. Overall, the railway line is characterized by a low wind energy environment ($DP \leq 200$ VU), and the directional variability index is moderate ($0.3 < RDP/DP < 0.8$). Sand materials are primarily fine sand (2–3 Φ) and medium sand (1–2 Φ). The key period for wind-sand hazard prevention and control is spring. In the Zhangda and Deji sections, the angle between the wind-sand transport direction and the railway direction is small, resulting in a low hazard level. Special sand control measures are unnecessary, but efforts should focus on ecological protection and vegetation restoration through closure and cultivation. In contrast, the Xierong and Jiabang sections exhibit a large angle between the wind-sand transport direction and the railway, posing a significant hazard. In these sections, wind-sand prevention and control should focus on blocking (sand) and consolidating (sand), using external barriers and internal consolidation (distant

blocking and near consolidation). Simultaneously, sand-fixing vegetation should be cultivated to establish a comprehensive protection system.

Data availability

All data generated or analysed during this study are included in this published article.

Received: 7 April 2025; Accepted: 25 September 2025
Published online: 31 October 2025

References

1. Yao, J. M. et al. Characteristics of a rapid landsliding area along Jinsha river revealed by multi–temporal remote sensing and its risks to Sichuan–Tibet railway. *Landslides* **19**, 703–718 (2022).
2. Lu, C. F. & Cai, C. X. Challenges and countermeasures for construction safety during the Sichuan–Tibet railway project. *Engineering* **5** (5), 833–838 (2019).
3. Yang, J. H. et al. Near–surface wind environment in the Yarlung Zangbo river basin, Southern Tibetan plateau. *J. Arid Land.* **12** (6), 917–936 (2020).
4. Zhang, J. Q., Zhang, C. L., Li, Q. & Pan, X. H. Grain-size distribution of surface sediments of climbing and falling dunes in the Zedang Valley of the Yarlung Zangbo River, Southern Tibetan plateau. *J. Earth Syst. Sci.* **128** (1), 11 (2019).
5. Zhou, N., Zhang, C. L., Wu, X. X., Wang, X. M. & Kang, L. Q. The geomorphology and evolution of aeolian landforms within a river Valley in a semi–humid environment: A case study from Mainling Valley. *Qinghai–Tibet Plateau Geomorphology*. **224**, 27–38 (2014).
6. Shen, W. S., Li, H. D., Sun, M. & Jiang, J. Dynamics of aeolian sandy land in the Yarlung Zangbo river basin of Tibet, China from 1975 to 2008. *Glob Planet. Change*. **86–87**, 37–44 (2012).
7. Zou, X. Y. et al. Desertification and control plan in the Tibet autonomous region of China. *J. Arid Environ.* **51**, 183–198 (2002).
8. Dong, G. R. et al. The causes and developmental trend of desertification in the middle reaches of the Yarlung Zangbo river and its two tributaries in Xizang. *Chin. Geogr. Sci.* **5** (4), 355–364 (1995).
9. Liu, Y., Wang, Y. S. & Shen, T. Spatial distribution and formation mechanism of aeolian sand in the middle reaches of the Yarlung Zangbo river. *J. Mt. Sci.* **16** (9), 1987–2000 (2019).
10. Stauch, G. Geomorphological and palaeoclimate dynamics recorded by the formation of aeolian archives on the Tibetan plateau. *Earth-Sci. Rev.* **150**, 393–408 (2015).
11. Li, S. et al. Formation mechanism and development pattern of aeolian sand landform in Yarlung Zangbo river Valley. *Sci. China Ser. D-Earth Sci.* **42** (3), 272–284 (1999).
12. Dong, M. et al. Morphological characteristics and dynamic changes of typical climbing dunes on the Qinghai–Tibet plateau. *Geomorphology* **440**, 108869 (2023).
13. Dong, M. et al. Distribution patterns and morphological classification of climbing dunes in the Qinghai–Tibet plateau. *Aeolian Res.* **35**, 58–68 (2018).
14. Shi, X. N. et al. Spatiotemporal variations of suspended sediment transport in the upstream and midstream of the Yarlung Tsangpo river (the upper Brahmaputra), China. *Earth Surf. Process. Landf.* **43** (2), 432–443 (2018).
15. Dong, Z. B. et al. High–altitude aeolian research on the Tibetan plateau. *Rev. Geophys.* **55** (4), 864–901 (2017).
16. Minola, L. et al. Climatology of near–surface wind speed from observational, reanalysis and high–resolution regional climate model data over the Tibetan plateau. *Clim. Dyn.* **62**, 933–953 (2024).
17. Xie, S. B., Qu, J. J., Han, Q. J. & Pang, Y. J. Experimental definition and its significance on the minimum safe distance of blown sand between the proposed Qinghai–Tibet expressway and the existing Qinghai–Tibet railway. *Sci. China-Technol Sci.* **63** (12), 2664–2676 (2020).
18. Huang, N. et al. Investigations into the law of sand particle accumulation over railway subgrade with wind–break wall. *Eur. Phys. J. E.* **42** (11), 145 (2019).
19. Bruno, L., Horvat, M. & Raffaele, L. Windblown sand along railway infrastructures: A review of challenges and mitigation measures. *J. Wind Eng. Ind. Aerodyn*. **177**, 340–365 (2018).
20. Zhang, K. C., Zhang, H. X., An, Z. S. & Xue, C. J. Evaluation of windproof and sand fixation effect of protective system in the desert Oasis ecotone of Mingsha mountain Dunhuang. *Sci. Rep.* **15** (1), 546 (2025).
21. Xue, C. J. et al. Effect of Bridge height on airflow and aeolian sand flux near surface along the Qinghai–Tibet Railway, China. *Sci. Rep.* **14** (1), 15990 (2024).
22. Fryberger, S. G. & Dean, G. Dune forms and wind regime. In: (ed Mckee, E.) D. A Study of Global Sand Seas, U.S. Geological Survey Professional Papers 1052, University Press of the Pacific, Honolulu, HI, USA, 137–169 (1979).
23. Ling, Y. Q. Engineering calculation of maximum possible sand transporting quantity. *J. Desert Res.* **17** (4), 362–368 (1997). (in Chinese with English Abstract).
24. Xie, S. B., Qu, J. J., Pang, Y. J., Zhang, K. C. & Wang, C. Dynamic mechanism of blown sand hazard formation at the Jieqiong section of the Lhasa–Shigatse railway. *Geomat. Nat. Hazards Risk*. **12** (1), 153–165 (2021).
25. Xie, S. B., Zhang, X., Pang, Y. J. & Zhang, K. Y. Blown sand environment characteristics and Bridge sand hazard mechanisms of expressways in the South Tibet Valley. *Sci. Rep.* **14** (1), 24665 (2024).
26. Lai, W. et al. Grain–size and compositional variability of Yarlung Tsangpo sand (Xigaze transect, South Tibet): implications for sediment mixing by fluvial and aeolian processes. *J. Palaegeogr*. **12** (2), 195–210 (2023).
27. Zhang, Z. C., Ma, P. F., La, Z., Zhang, Y. & Liang, A. M. Aeolian sediment provenance and transport in the upper and middle reaches of the Yarlung Zangbo River, Tibet plateau. *Basin Res.* **35** (2), 762–783 (2023).
28. Lu, J. X., Liu, Y. D., Wang, X. L., Chen, J. B. & Ding, G. D. Wind regime and sand drift potential characteristics in the Milin section along arid Valley of the Yarlung Zangbo river. *J. Arid Land. Resour. Environ.* **39** (04), 145–155 (2025). (in Chinese with English Abstract).
29. Ma, P. F. et al. Analysis on the sand transport wind power conditions and suggestions on the sand disaster preventions in the middle reaches of Yarlung Zangbo River,China. *J. Desert Res.* **41** (01), 10–18 (2021). (in Chinese with English Abstract).
30. Liu, Y., Wang, Y. S. & Shen, T. Spatial distribution and formation mechanism of aeolian sand in the middle reaches of the Yarlung Zangbo river. *J. Mt. Sci.* **16** (09), 1987–2000 (2019).
31. Yang, J. H. et al. Near-surface wind environment in the Yarlung Zangbo river basin, Southern Tibetan plateau. *J. Arid Land.* **12** (06), 917–936 (2020).
32. Zhang, L. G. et al. The Spatial variations of sand drift potential in Yarlung Zangbo river basin. *J. Desert Res.* **45** (01), 304–317 (2025). (in Chinese with English Abstract).
33. Wang, X. M. & Chen, G. T. Efficiencies and reasonable width for the mechanical sand–prevention system along the Tarim desert highway. *J. Arid Land. Resour. Environ.* **11** (4), 28–35 (1997). (in Chinese with English Abstract).
34. Li, S. Y., Wang, D. & Lei, J. Q. Spatial distribution of sand drift disasters on road surface in the hinterland of the Taklimakan desert. *Arid Land. Geogr.* **28** (1), 93–97 (2005). (in Chinese with English Abstract).

35. Zhang, X., Xie, S. B. & Pang, Y. J. Numerical simulation on wind–sand flow field around railway embankment with different wind angles. *Front. Environ. Sci.* **10**, 1073257 (2023).

Acknowledgements
This research project was supported by the National Natural Science Foundation of China (Grant No. 42477505), the Western Young Scholars project of the Chinese Academy of Sciences of China (Grant No. XBZGLZB2022024), the Natural Science Foundation of Gansu Province for Distinguished Young Scholars (Grant No. 22JR5RA049), and the Longyuan Youth Talent Project of Gansu Province (Grant No. E339020101).

Author contributions
Shengbo Xie designed the study and wrote the manuscript, Keying Zhang and Xian Zhang analyzed the data and revised the manuscript, Kecun Zhang participated in the experiment. All authors discussed the results and contributed to the manuscript.

Declarations

Competing interests
The authors declare no competing interests.

Additional information
Correspondence and requests for materials should be addressed to S.X.

Reprints and permissions information is available at www.nature.com/reprints.

Publisher's note Springer Nature remains neutral with regard to jurisdictional claims in published maps and institutional affiliations.